ACS APPLIED MATERIALS & INTERFACES

Research Article

www.acsami.org

Realization of Cu-Doped p-Type ZnO Thin Films by Molecular Beam Epitaxy

Mohammad Suja, Sunayna B. Bashar, Muhammad M. Morshed, and Jianlin Liu*

Department of Electrical and Computer Engineering, University of California, Riverside, California 92521, United States

Supporting Information

ABSTRACT: Cu-doped p-type ZnO films are grown on c-sapphire substrates by plasma-assisted molecular beam epitaxy. Photoluminescence (PL) experiments reveal a shallow acceptor state at 0.15 eV above the valence band edge. Hall effect results indicate that a growth condition window is found for the formation of p-type ZnO thin films, and the best conductivity is achieved with a high hole concentration of 1.54×10^{18} cm^{-3}, a low resistivity of 0.6 Ω cm, and a moderate mobility of 6.65 $cm^2 V^{-1} s^{-1}$ at room temperature. Metal oxide semiconductor capacitor devices have been fabricated on the Cu-doped ZnO films, and the characteristics of capacitance−voltage measurements demonstrate that the Cu-doped ZnO thin films under proper growth conditions are p-type. Seebeck measurements on these Cu-doped ZnO samples lead to positive Seebeck coefficients and further confirm the p-type conductivity. Other measurements such as X-ray diffraction, X-ray photoelectron, Raman, and absorption spectroscopies are also performed to elucidate the structural and optical characteristics of the Cu-doped p-type ZnO films. The p-type conductivity is explained to originate from Cu substitution of Zn with a valency of +1 state. However, all p-type samples are converted to n-type over time, which is mostly due to the carrier compensation from extrinsic defects of ZnO.

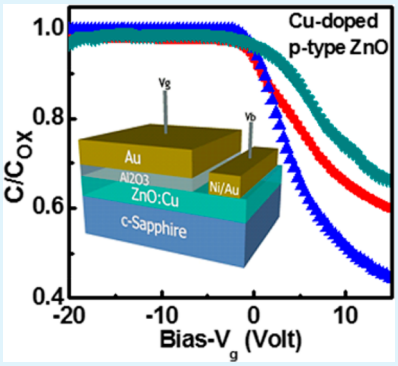

KEYWORDS: *ZnO, Cu dopant, p-type, molecular beam epitaxy (MBE), thin film*

1. INTRODUCTION

Having a wide band gap of 3.37 eV at room temperature, zinc oxide (ZnO) has been recognized as a promising material for near ultraviolet (UV) optoelectronic devices ever since its p-type conductivity was demonstrated.[1−9] In addition, the large exciton binding energy (60 meV) of ZnO at room temperature (RT) generates the interesting possibility of utilizing excitonic effects in RT optoelectronic devices.[10,11] However, the major challenge for the fabrication of robust and long-lasting optoelectronic devices lies in achieving high-quality and highly stable p-type ZnO.

Many research groups have been working over the decades to search for stable and reproducible p-type ZnO. p-Type doping in ZnO may be possible by substituting either group IA elements (Li, Na, and K) for Zn sites or group V elements (N, P, As, and Sb) for O sites.[12] Group IA elements tend to occupy the interstitial sites rather than substitutional sites because their ionic radii are smaller than that of Zn, which makes it difficult to produce p-type materials.[13] On the other hand, even though there are many reports on successful p-doping using group V elements,[3,14−19] the reproducibility and reliability of these results are still under constant debate,[20] as the origin of p-type may not be from direct substitution of these group V elements on the O sites but from defect complexes.[21] Because of the limitations of group IA and V elements, recently several groups have focused on group IB elements (Cu, Ag, and Au), especially Ag, for p-type doping.[22−27] From the first-principles calculations of doping effects with group IB elements, the formation energies on the substitutional sites are very low compared to that on the interstitial sites under oxygen-rich growth conditions, which suppress the formation of major hole-killer defects such as oxygen vacancies and Zn interstitials.[28] Therefore, the group IB elements could act as an acceptor in ZnO, if incorporated on substitutional Zn sites.[29] Fan and Freer suggested that Ag can exist both on substitutional Zn sites (Ag_{Zn}) and in the interstitial sites (Ag_i).[30] On the other hand, there have been very few reports regarding Cu-doping of epitaxial ZnO. Mollwo et al. reported the existence of an energy level of the Cu^{2+} atoms located 0.19 eV below the conduction band edge for Cu/In codoped ZnO.[31] Later, Kanai also reported that Cu^{2+} level is located 0.17 eV below the bottom of the conduction band as Cu atom substitutes at the Zn site.[32] Recently, Xu et al. reported that Cu doping introduces an acceptor (Cu^+) level in ZnO at 0.45 eV above the valence band.[33] One can conclude from these reports that Cu may assume a valency of either +1 or +2 depending on its chemical environment, for example, in the compounds Cu_2O and CuO, respectively. However, whether and how Cu doping can lead to p-type ZnO remains unclear.

We report on molecular beam epitaxial (MBE) growth and characterization of Cu-doped ZnO thin films. Photoluminescence (PL), Hall effect, Seebeck effect, capacitance−voltage,

Received: February 17, 2015
Accepted: April 1, 2015
Published: April 2, 2015

DOI: 10.1021/acsami.5b01564
ACS Appl. Mater. Interfaces 2015, 7, 8894−8899

etc. were used to assess the films. A growth window of Cu doping to achieve p-type ZnO thin films is demonstrated. Shallow acceptors with an activation energy of 0.15 eV are proven. Strong p-type conductivity with room-temperature hole concentration exceeding 1×10^{18} cm^{-3} is demonstrated.

2. EXPERIMENTAL SECTION

2.1. Cu-Doped ZnO Thin-Film Growth. Cu-doped ZnO thin films were grown on c-sapphire substrates using an SVTA radio frequency (RF) plasma-assisted MBE system. Radical Knudsen effusion cells filled with elemental Zn (6N), Mg (6N), and Cu (6N) metals were used as Zn, Mg, and Cu sources. Zn, Mg, and Cu fluxes were controlled by the effusion cell temperatures. O_2 (6N) gas was fed through the RF plasma generator used as the oxygen source, and the oxygen flow rate was precisely tuned by a mass flow controller. The substrates were cleaned in an aqua regia (HNO_3: HCl = 1:3) solution at 150 °C for 20 min before deionized (DI) water rinsing and blow drying by nitrogen. These substrates were then immediately transferred to the MBE chamber. During the growth, several steps were followed. In step I, the substrate was annealed in vacuum at 800 °C for 15 min to create an atomically smooth substrate surface. In step II, an MgO/MgZnO/ZnO low-temperature buffer layer was grown at 450 °C for 5 min with an estimated total thickness of 2−3 nm. In step III, another low-temperature ZnO buffer layer was grown at 500 °C for 10 min. During the growth of buffer layers, Zn and Mg cell temperature were kept at 320 and 470 °C respectively. Oxygen flow rate was 3 sccm with 400 W plasma power. The buffer layers minimize the lattice mismatch between Cu-doped ZnO and c-sapphire substrate. In step IV, the Cu-doped ZnO films were grown at 600 °C on top of the buffer layer for 3 h with Zn cell temperature and O_2 flow rate at 340 °C and 2 sccm, respectively. Cu effusion cell temperature was adjusted from 610 to 590 °C with an interval of 5 °C for samples A−E, as summarized in Table 1. In step V, an in situ annealing was performed at 650 °C for 20 min with 1 sccm of O_2 flow to activate the Cu dopants. The total thickness of the films was about 400 nm.

Table 1. Growth Conditions for Samples A−E[a]

sample	heater temperature (°C)	Zn cell temperature (°C)	Cu Cell Temperature (°C)	O_2 flux (sccm)	growth duration (h)
A	500	340	610	2	3
B	500	340	605	2	3
C	500	340	600	2	3
D	500	340	595	2	3
E	500	340	590	2	3

[a]A growth window of p-type Cu-doped ZnO films (samples B−D) is identified.

2.2. Structural, Optical, Electrical, and Seebeck Characterization. The thickness of the films were measured using a Dektak 8 surface profilometer. X-ray diffraction measurement was performed using a Bruker D8 Advance X-ray diffractometer. A Horiba LabRam Raman spectroscopy system was used to investigate Raman spectrum of the Cu-doped ZnO samples. Absorption spectra were measured by a Varian Cary 500 double-beam scanning ultraviolet/visible/near-infrared (UV/vis/NIR) spectrophotometer. PL study was carried out using a home-built PL system with a Janis cryostat, a 325 nm He−Cd laser for the excitation source, and a photomultiplier tube. Room-temperature Hall effect measurement was done in a variable magnetic field up to 6000 gauss. For Hall measurement system, a Keithley 6220 current source and a Keithley 2182 voltmeter were used with minimum current capability of 0.1 pA, up to 105 V compliance, and voltage capability of 1 nV, respectively. Au/Ni (100 nm/10 nm) was deposited for Hall bar geometry sample as the metal contacts and also annealed properly using the rapid thermal annealing process. A home-built heater and heat sink system, together with a Keithley 2401 digital multimeter, were used to measure the voltage and temperature for Seebeck measurements.

2.3. MOS Device Fabrication and Characterization. A square geometry (200×200 μm^2) MOS capacitor device was fabricated using a standard photolithography process. An aluminum oxide (Al_2O_3) layer of 30 nm was deposited on the Cu-doped ZnO films by an atomic layer deposition (ALD) process. Au (200 nm) was deposited on both Al_2O_3 and Cu-doped ZnO films as the contacts for metal and semiconductor by an electron beam evaporation process. The capacitance was measured using an Agilent 4284A LCR meter.

3. RESULTS AND DISCUSSION

Table 1 summarizes the growth conditions of Cu-doped ZnO samples. All five samples adopted the same growth temperature of 500 °C, Zn cell temperature of 340 °C, oxygen flow rate at 2 sccm, and growth time of 3 h. The only variable parameter is the Cu effusion cell temperature. The electrical properties of the films are summarized in Table 2 with the date measured. Sample A, which was grown at a Cu cell temperature of 610 °C, shows n-type conductivity with a carrier concentration of 8.3×10^{17} cm^{-3} and a mobility of 12.48 $cm^2 V^{-1} s^{-1}$. With a Cu cell temperature of 605 °C (sample B), the film exhibits p-type behavior with a hole concentration of 2.9×10^{17} cm^{-3} and a mobility of 32.89 $cm^2 V^{-1} s^{-1}$. By decreasing the Cu cell temperature to 600 °C (sample C), the carrier concentration increases to 1.54×10^{18} cm^{-3} with a mobility of 6.65 $cm^2 V^{-1} s^{-1}$. Further decrease of the Cu cell temperature to 595 °C (sample D) leads to the decrease of hole carrier concentration to 1.22×10^{17} cm^{-3} with a lower mobility of 0.59 $cm^2 V^{-1} s^{-1}$. As the Cu cell temperature reaches 590 °C (sample E), the film behavior is n-type. Therefore, an approximate p-type ZnO growth window is identified with the Cu effusion cell temperature between 595 and 605 °C. Sample C′ represents the sample C that turns into n-type after 5 months. Because all p-type samples converted into n-type after about 5 months, only the electrical property data of the representative sample C′ is included in Table 2 to avoid redundancy.

3.1. Structural and Optical Characterizations. Figure 1a shows an X-ray diffraction (XRD) spectrum of Cu-doped ZnO film (sample C). The spectrum exhibits diffraction peaks for ZnO(0002) and Al_2O_3(0006). The absence of other ZnO directions indicates that the ZnO film is single-crystalline in

Table 2. Results of RT Hall Measurements of Cu-Doped ZnO Films[a]

sample	date measured	carrier concentration (cm^{-3})	mobility ($cm^2 V^{-1} s^{-1}$)	resistivity (Ω cm)	electrical type
A	05/05/2014	8.3×10^{17}	12.48	0.60	n-type
B	05/07/2014	2.9×10^{17}	32.89	0.65	p-type
C	05/09/2014	1.54×10^{18}	6.65	0.61	p-type
D	05/10/2014	1.22×10^{17}	0.59	87.5	p-type
C′	10/20/2014	6.39×10^{17}	16.56	0.59	n-type

[a]Sample C′ represents sample C measured after 5 months.

DOI: 10.1021/acsami.5b01564
ACS Appl. Mater. Interfaces 2015, 7, 8894−8899

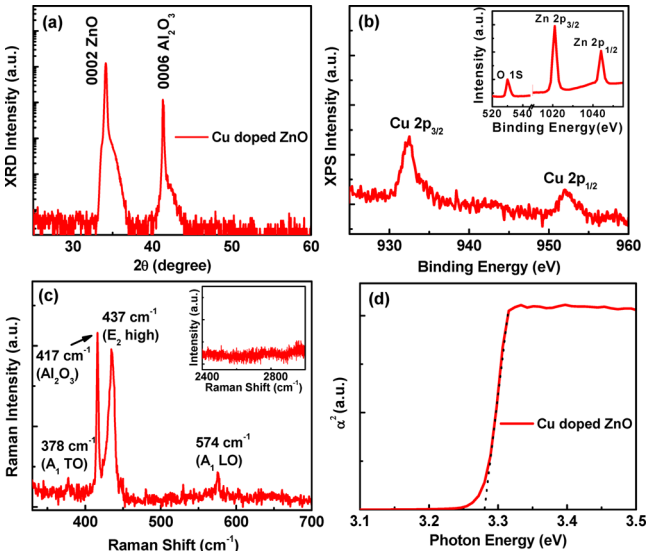

Figure 1. (a) XRD spectrum of p-type Cu-doped ZnO (sample C), (b) Cu 2p core-level XPS spectrum of sample C (inset showing XPS spectrum for Zn 2p and O 1s), (c) Raman spectrum of Cu-doped ZnO (sample C; inset is Raman spectrum showing no Cu-rich secondary phases), and (d) square of absorption coefficient (α^2) at room temperature of sample C.

nature. Moreover, no diffraction signals originating from Cu and its compounds are observed within the detection level. Figure 1b shows a Cu 2p core level XPS spectrum of Cu-doped ZnO film (sample C) with an inset indicating peaks relative to Zn and O. The incorporation of Cu dopant is determined by two prominent peaks at 932.4 and 952 eV corresponding to Cu $2p_{3/2}$ and Cu $2p_{1/2}$ spin−orbit splitting, respectively. This result indicates that the incorporated Cu exists in the form of copper(I) oxide (Cu^+) in our Cu-doped ZnO film. Because copper(II) oxide (Cu^{2+}) has hole states in the Cu 3d band (Cu $3d^9$ configuration), strong satellite peaks are commonly found between 940 and 945 eV because of electron shakeup.[34] Whereas the 3d band of copper(I) oxide (Cu^+) is filled (Cu $3d^{10}$), the 4s band is unoccupied; thus, no satellites are expected, which is in accordance with our result. The XPS spectrum of sample C′ is shown in the Supporting Information (Figure S1). All peaks corresponding to Zn, O, and Cu elements resemble their original peaks in Figure 1b, suggesting that the change of the conductivity originates from extrinsic factors, as discussed later. Figure 1c shows Raman spectrum of Cu-doped ZnO film (sample C). According to group theory, the following fundamental optical modes should exist in a wurtzite ZnO: E_2 (low) at 101 cm^{-1}, E_2 (high) at 437 cm^{-1}, A_1 (TO) at 380 cm^{-1}, A_1 (LO) at 574 cm^{-1}, E_1 (TO) at 407 cm^{-1}, and E_1 (LO) at 583 cm^{-1}. The low-frequency E_2 mode is associated with the vibration of the heavy Zn sublattice, while the high-frequency E_2 mode involves only the oxygen atoms.[35−37] From the Raman spectrum of Cu-doped ZnO film, a strong Raman shift signal appears at 437 cm^{-1} because of the E_2 (high) mode of ZnO along with weak peaks at 378 and 574 cm^{-1}, which correspond to A_1 (TO) and A_1 (LO) modes of ZnO, respectively. The peak at 417 cm^{-1} is attributed to the optical phonon mode of the c-sapphire substrate. As seen from the inset, there is no signal corresponding to copper oxide or other copper compounds in the Raman spectrum, which is consistent with the XRD results that no secondary phases are present in the Cu-doped ZnO film. Figure 1d shows the derived spectrum of α^2 versus photon energy ($h\nu$) of sample C at room temperature, where α is the absorption coefficient. By utilizing the Tauc's plot, a direct band gap of 3.28 eV (378 nm) is obtained by taking the intercept of the extrapolation to the zero absorption. The excitonic resonance peak in the spectrum shows good optical quality and the single slope absorption edge ensures no significant phase mixing in the film.

3.2. Photoluminescence Experiments. Figure 2a shows room-temperature PL spectra of samples A−D. The near band

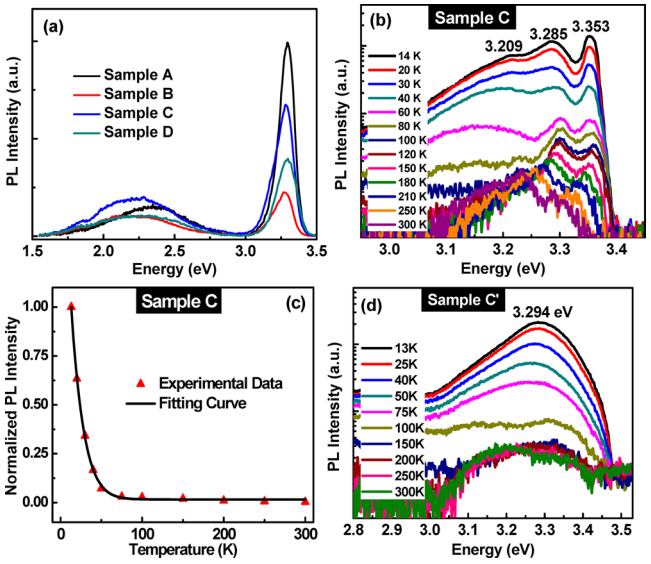

Figure 2. (a) Room-temperature PL spectra of Cu-doped ZnO samples (samples A−D), (b) temperature-dependent PL spectra of p-type Cu:ZnO sample C, (c) integrated intensity of the A°X emission as a function of temperature for sample C. The triangles represent the experimental data, and the solid line is the fitting to eq 2. Panel d provides the temperature-dependent PL spectra of sample C′.

edge (NBE) emission at about 3.27 eV (380 nm) and a weak broad green emission (GE) centered at about 2.25 eV (550 nm) can be observed from the Cu-doped p-type ZnO films (samples B−D). For Cu-doped ZnO film outside the p-type growth window (sample A), the GE center shifts toward shorter wavelength (~2.30 eV). The NBE emission results from exciton-related recombination.[38,39] The green emission might originate from intrinsic defects and/or Cu dopants. The origin of GE in undoped ZnO has been investigated extensively and explained by different types of electron transitions such as from oxygen vacancy (V_O) donor level to the valence band (D−h), from V_O to deep Zn vacancy (V_{Zn}) acceptor level (DAP), from the conduction band to the V_{Zn} acceptor level (e−A), and between two states of V_O (intracenter).[40] In the case of Cu-doped ZnO, Gruzintsev et al. reported that visible emission observed at around 2.27 eV corresponds to DAP transitions from V_O to Cu_{Zn} levels of Cu^+:$3d^{10}$.[41] Because our Cu-doped p-type ZnO thin films (samples B−D) were grown in O-rich conditions and annealed in an O-plasma environment, oxygen interstitial (O_i) and V_{Zn} should have dominant concentration.[42] Therefore, the GE peak of 2.25 eV is more probably due to the transition between O_i level and conduction band.

Figure 2b shows temperature-dependent PL spectra of sample C measured from 14 to 300 K. Similar temperature-dependent PL spectra of other p-type samples (samples B and D) are shown in the Supporting Information (Figure S2). For Cu-doped p-type ZnO films (samples B−D), the NBE

DOI: 10.1021/acsami.5b01564
ACS Appl. Mater. Interfaces 2015, 7, 8894−8899

emissions associated with acceptor bound exciton (A°X) are observed at 3.350−3.353 eV. With an increase of the temperature from 14 to 80 K, emissions of 3.285 and 3.209 eV observed at 14 K show blue shifts, which are typical characteristics of FA and DAP transitions.[43] Over the entire temperature range, the 3.285 eV emission line progressively merges into the 3.209 eV emission line, showing the feature of the thermal ionization of donors.[44] Therefore, these two emissions at 3.285 and 3.209 eV are identified as FA and DAP transitions, respectively. The acceptor activation energy, E_A, can be calculated from eq 1.[15,43]

$$E_A = E_{gap} - E_{FA} + k_B T/2 \quad (1)$$

where the temperature-dependent transition E_{FA} is approximately 3.285 eV at 14 K and the intrinsic band gap E_{gap} is about 3.43 eV at 14 K.[44] Therefore, the value of E_A is calculated to be 0.15 eV. Figure 2c shows the integrated intensity of the A°X emission of sample C as a function of temperature. The temperature dependence of the integrated PL intensity can be described by eq 2.[45]

$$I(T) = I_0 \Big/ \left[1 + C \exp\left(-\frac{E_b^{A°X}}{kT}\right)\right] \quad (2)$$

where $E_b^{A°X}$ is the binding energy of the acceptor and free exciton, C a fitting parameter, and I_0 the integrated PL intensity at zero temperature, which is approximately the same as that at T = 14 K. From the fitting to eq 2, $E_b^{A°X}$ = 17 meV is obtained. If an Haynes factor $((E_b^{A°X})/(E_A)) \approx 0.1$ is used,[46] acceptor binding energy, E_A, is estimated to be 0.17 eV. This result is in close agreement with the value estimated above from spectroscopic data using eq 1. On the other hand, if we assume that the acceptor activation energy is 0.15 eV, the Haynes factor for Cu-doped ZnO is estimated to be about 0.113, which is comparable with the value for Sb-doped ZnO.[46]

Figure 2d shows temperature-dependent PL spectra of sample C after it converts to n-type over time (denoted as sample C′). The spectra have noticeably changed. A broad emission is observed at 3.294 eV at 14 K and redshifts with the increase of temperature for sample C′. This suggests that the spectra are now dominated by donor-bound exciton emissions. Because the sample was stored in the ambient air, hydrogen-related impurities may absorb and diffuse into the ZnO, which contribute to a great deal of donors. These donors eventually compensate Cu-induced holes, leading to the conversion of the conductivity type.

3.3. Electrical Characterization: Hall Experiments and MOS Device Fabrication. Figure 3 shows Hall resistance as a function of magnetic field at room temperature for the samples. Positive increase in Hall resistance with applied magnetic field is observed in samples B−D, demonstrating p-type conductivity of these samples. Sample C has the most positive slope, which supports its higher carrier concentration value compared with that of others. The negative sloped lines for samples A and C′ represent the n-type conductivity of these samples.

MOS devices were fabricated to further study the p-type behavior of Cu-doped ZnO samples. The inset of Figure 4 shows the device structure, consisting of a metal gate (Au, 200 nm), Al_2O_3 (30 nm), and Cu-doped ZnO film (400 nm) on c-sapphire substrate. Capacitance−voltage (C−V) curves were measured at 300 K with a frequency of 100 kHz. For samples

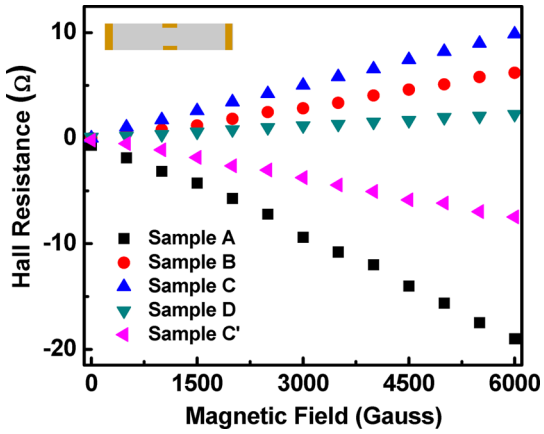

Figure 3. RT Hall resistance as a function of applied magnetic field of various Cu-doped ZnO films. Inset shows one of the fabricated samples used for Hall effect measurement.

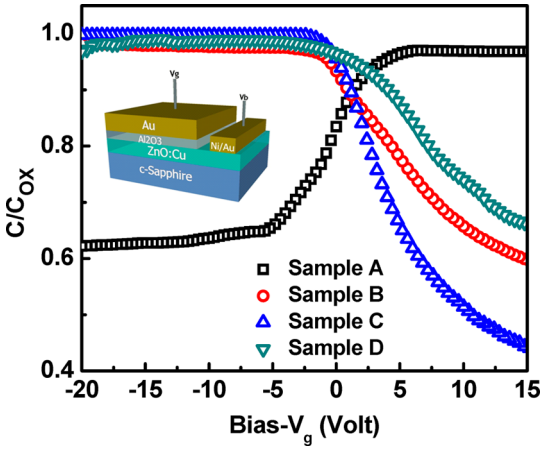

Figure 4. C−V characteristics of fabricated MOS capacitor (inset) devices utilizing Cu-doped ZnO (samples A−D) as the semiconductor layer, Al_2O_3 as the oxide layer, and Au as the metal layer.

B−D, by increasing the gate voltage from negative to positive values, the p-type Cu-doped ZnO film can accumulate holes (accumulation mode), then deplete holes (depletion mode), and finally fill with electrons on top of the Cu-doped ZnO film (inversion mode). In contrast, for sample A, by decreasing the gate voltage from positive to negative values, the n-type film can accumulate electrons (accumulation mode), then deplete electrons (depletion mode), and finally fill with holes on top of the Cu-doped ZnO film (inversion mode). These trends of C−V curves further demonstrate the p-type conductivity of Cu-doped ZnO films.

3.4. Seebeck Characterization. Figure 5 shows Seebeck effect measurement results. The decrease in voltage with the increase in temperature difference confirms the n-type conductivity of sample A. Positive increase in voltage with the increase in temperature difference is evident for samples B−D, which confirms their p-type conductivity. The most positive slope is observed in sample C, which indicates its carrier concentration is higher than that of other p-type samples (samples B and D).

3.5. Discussion. Finally, we briefly discuss the origin of the Cu-doped p-type ZnO. Owing to similar ionic radii between Cu and Zn, and low formation energy of group IB elements to occupy substitutional Zn site, Cu mostly substitutes Zn atom in

DOI: 10.1021/acsami.5b01564
ACS Appl. Mater. Interfaces 2015, 7, 8894−8899

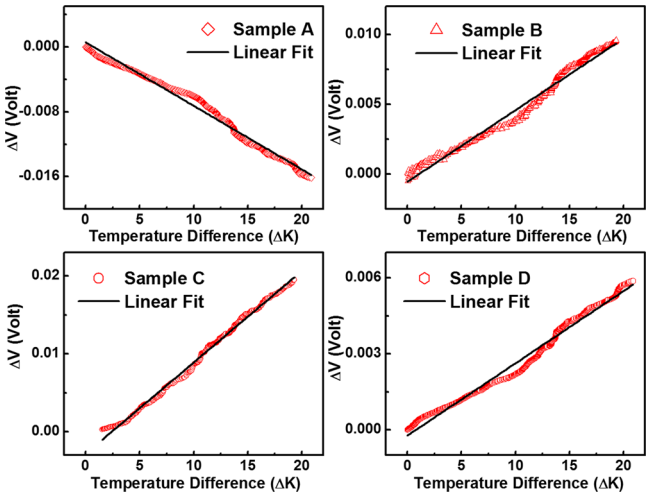

Figure 5. Variation in voltage with temperature difference for various Cu-doped ZnO samples (samples A–D).

Cu-doped ZnO films.[28] Because of proper O-rich conditions, these Cu atoms appear as a valency of +1 state, as revealed by XPS results. These Cu^+ ions create a shallow acceptor level at 0.15 eV above the valence band indicated from PL studies, which is responsible for p-type conductivity in our Cu-doped ZnO films within a Cu effusion cell temperature window. Because the Cu-doped ZnO films were grown in O-rich conditions, the density of intrinsic donors has been minimized. Nevertheless, there are still some extrinsic donors originating from hydrogen-related complexes and other possible alien impurities during the growth; therefore, the Cu cell temperature must be raised to a point where Cu^+ concentration is high enough to compensate these inadvertent donors to result in p-type conductivity. The dopant compensation can be clearly inferred from DAP emissions in PL studies. As the Cu cell temperature exceeds the upper bound of the p-type film growth window, ZnO becomes n-type. This behavior may be explained by the nature of Cu doping in ZnO film. Because Cu^+ and Cu^{2+} atoms can coexist in ZnO and as more Cu atoms are incorporated into ZnO at a higher Cu cell temperature, Cu^{2+} atoms may outnumber Cu^+ atoms. These excess Cu^{2+} atoms have a tendency to form deep donor levels, resulting in the disappearance of p-type conductivity.[31,32,34]

4. CONCLUSION

Cu-doped p-type ZnO thin films were grown by MBE with an incorporation of a proper number of Cu atoms and comprehensively characterized by a combination of Hall effect, Seebeck effect, and $C-V$ for the first time. A range of p-type conductivity was observed in the Cu-doped ZnO films with the strongest p-type behavior exhibiting a hole concentration of 1.54×10^{18} cm^{-3}, a resistivity of 0.6 Ω cm, and a mobility of 6.65 $cm^2 V^{-1} s^{-1}$ at room temperature. PL studies revealed a shallow acceptor energy level of 0.15 eV above the valence band. The p-type behavior was found to originate from cationic substitution at the Zn site with Cu^+ state. Although the stability of Cu-doped p-type ZnO films remains an issue, our experimental results indicate that Cu could be an excellent candidate for p-type ZnO fabrication.

■ ASSOCIATED CONTENT

Supporting Information

XPS spectrum of sample C′ and temperature-dependent PL of p-type Cu-doped ZnO samples B and D. This material is available free of charge via the Internet at http://pubs.acs.org.

■ AUTHOR INFORMATION

Corresponding Author

*E-mail: jianlin@ece.ucr.edu.

Notes

The authors declare no competing financial interest.

■ ACKNOWLEDGMENTS

The authors acknowledge the financial support from the Department of Energy (DE-FG02-08ER-46520).

■ REFERENCES

(1) Bagnall, D. M.; Chen, Y. F.; Zhu, Z.; Yao, T.; Koyama, S.; Shen, M. Y.; Goto, T. Optically Pumped Lasing of ZnO at Room Temperature. *Appl. Phys. Lett.* **1997**, *70*, 2230–2232.

(2) Zu, P.; Tang, Z. K.; Wong, G. K. L.; Kawasaki, M.; Ohotomo, A.; Koinuma, H.; Segawa, Y. Ultraviolet Spontaneous and Stimulated Emissions from ZnO Microcrystallite Thin Films at Room Temperature. *Solid State Commun.* **1997**, *103*, 459–463.

(3) Ryu, Y. R.; Zhu, S.; Look, D. C.; Wrobel, J. M.; Jeong, H. M.; White, H. W. Synthesis of p-Type ZnO Films. *J. Cryst. Growth* **2000**, *216*, 330–334.

(4) Choopun, S.; Vispute, R. D.; Noch, W.; Balsamo, A.; Sharma, R. P.; Venkatesan, T.; Iliadis, A.; Look, D. C. Oxygen Pressure-Tuned Epitaxy and Optoelectronic Properties of Laser-Deposited ZnO Films on Sapphire. *Appl. Phys. Lett.* **1999**, *75*, 3947–3949.

(5) Wong, E. M.; Searson, P. C. ZnO Quantum Particle Thin Films Fabricated by Electrophoretic Deposition. *Appl. Phys. Lett.* **1999**, *74*, 2939–2941.

(6) Ko, H. J.; Chen, Y. F.; Zhu, Z.; Yao, T.; Kobayashi, I.; Uchiki, H. Photoluminescence Properties of ZnO Epilayers Grown on CaF_2 (111) by Plasma Assisted Molecular Beam Epitaxy. *Appl. Phys. Lett.* **2000**, *76*, 1905–1907.

(7) Ogata, K.; Sakurai, K.; Fujita, Sz.; Fujita, Sg.; Matsushige, K. Effects of Thermal Annealing of ZnO Layers Grown by MBE. *J. Cryst. Growth* **2000**, *214*, 312–315.

(8) Pearton, S. J.; Norton, D. P.; Ip, K.; Heo, Y. W.; Steiner, T. Recent Advances in Processing of ZnO. *J. Vac. Sci. Technol., B* **2004**, *22*, 932–948.

(9) Look, D. C. Recent Advances in ZnO Materials and Devices. *Mater. Sci. Eng., B* **2001**, *80*, 383–387.

(10) Chu, S.; Wang, G.; Zhou, W.; Lin, Y.; Chernyak, L.; Zhao, J.; Kong, J.; Li, L.; Ren, J.; Liu, J. Electrically Pumped Waveguide Lasing from ZnO Nanowires. *Nat. Nanotechnol.* **2011**, *6*, 506–510.

(11) Yu, S. F.; Yuen, C.; Lau, S. P.; Park, W. I.; Yi, G. C. Random Laser Action in ZnO Nanorod Arrays Embedded in ZnO Epilayers. *Appl. Phys. Lett.* **2004**, *84*, 3241–3243.

(12) Park, C. H.; Zhang, S. B.; Wei, S.-H. Origin of *p*-Type Doping Difficulty in ZnO: The Impurity Perspective. *Phys. Rev. B: Condens. Matter Mater. Phys.* **2002**, *66*, 073202-1–073202-3.

(13) Look, D. C.; Jones, R. L.; Sizelove, J. R.; Garces, N. Y.; Giles, N. C.; Halliburton, L. E. The Path to ZnO Devices: Donor and Acceptor Dynamics. *Phys. Status Solidi A* **2003**, *195*, 171–177.

(14) Tsukazaki, A.; Ohtomo, A.; Onuma, T.; Ohtani, M.; Makino, T.; Sumiya, M.; Ohtani, K.; Chichibu, S. F.; Fuke, S.; Segawa, Y.; Ohno, H.; Koinuma, H.; Kawasaki, M. Repeated Temperature Modulation Epitaxy for *p*-Type Doping and Light-Emitting Diode Based on ZnO. *Nat. Mater.* **2005**, *4*, 42–46.

(15) Ryu, Y. R.; Lee, T. S.; Leem, J. H.; White, H. W. Fabrication of Homostructural ZnO *p–n* Junctions and Ohmic Contacts to Arsenic-Doped *p*-Type ZnO. *Appl. Phys. Lett.* **2003**, *83*, 4032–4034.

DOI: 10.1021/acsami.5b01564
ACS Appl. Mater. Interfaces 2015, 7, 8894–8899

(16) Look, D. C.; Reynolds, D. C.; Litton, C. W.; Jones, R. L.; Eason, D. B.; Cantwell, G. Characterization of Homoepitaxial *p*-Type ZnO Grown by Molecular Beam Epitaxy. *Appl. Phys. Lett.* **2002**, *81*, 1830−1832.
(17) Lim, J. H.; Kang, C. K.; Kim, K. K.; Park, I. K.; Hwang, D. K.; Park, S. J. UV Electroluminescence Emission from ZnO Light-Emitting Diodes Grown by High-Temperature Radiofrequency Sputtering. *Adv. Mater. (Weinheim, Ger.)* **2006**, *18*, 2720−2724.
(18) Kim, K. K.; Kim, H. S.; Hwang, D. K.; Lim, J. H.; Park, S. J. Realization of p-Type ZnO Thin Films via Phosphorus Doping and Thermal Activation of The Dopant. *Appl. Phys. Lett.* **2003**, *83*, 63−65.
(19) Mandalapu, L. J.; Xiu, F. X.; Yang, Z.; Zhao, D. T.; Liu, J. L. p-Type Behavior from Sb-Doped ZnO Heterojunction Photodiodes. *Appl. Phys. Lett.* **2006**, *88*, 112108-1−112108-3.
(20) Look, D. C.; Claflin, B. P-Type Doping and Devices Based on ZnO. *Phys. Status Solidi B* **2004**, *241*, 624−630.
(21) Limpijumnong, S.; Zhang, S. B.; Wei, S. H.; Park, C. H. Doping by Large-Size-Mismatched Impurities: The Microscopic Origin of Arsenic- or Antimony-Doped p-Type Zinc Oxide. *Phys. Rev. Lett.* **2004**, *92*, 155504-1−155504-4.
(22) Kang, H. S.; Ahn, B. D.; Kim, J. H.; Kim, G. H.; Lim, S. H.; Chang, H. W.; Lee, S. Y. Structural, Electrical, and Optical Properties of p-Type ZnO Thin Films with Ag Dopant. *Appl. Phys. Lett.* **2006**, *88*, 202108-1−202108-3.
(23) Deng, R.; Zou, Y.; Tang, H. Correlation Between Electrical, Optical Properties and Ag^{2+} Centers of ZnO:Ag Thin Films. *Phys. B (Amsterdam, Neth.)* **2008**, *403*, 2004−2007.
(24) Rita, E.; Wahl, U.; Lopes, A. M. L.; Araujo, J. P.; Correia, J. G.; Alves, E.; Soares, J. C. Lattice Site and Stability of Implanted Ag in ZnO. *Phys. B (Amsterdam, Neth.)* **2003**, *340*, 240−244.
(25) Ahn, B. D.; Kang, H. S.; Kim, J. H.; Kim, G. H.; Chang, H. W.; Lee, S. Y. Synthesis and Analysis of Ag-Doped ZnO. *J. Appl. Phys.* **2006**, *100*, 093701-1−093701-6.
(26) Duan, L.; Lin, B.; Zhang, W.; Zhong, S.; Fu, Z. Enhancement of Ultraviolet Emissions from ZnO Films by Ag Doping. *Appl. Phys. Lett.* **2006**, *88*, 232110-1−232110-3.
(27) Duan, L.; Gao, W.; Chen, R.; Fu, Z. Influence of Post-Annealing Conditions on Properties of ZnO:Ag Films. *Solid State Commun.* **2008**, *145*, 479−481.
(28) Yanfa, Y.; Al-Jassim, M. M.; Wei, S. H. Doping of ZnO by Group-IB Elements. *Appl. Phys. Lett.* **2006**, *89*, 181912-1−181912-3.
(29) Klingshirn, C. *Semiconductor Optics*; Springer: Berlin, 1995.
(30) Fan, J.; Freer, R. The Roles Played by Ag and Al Dopants in Controlling the Electrical Properties of ZnO Varistors. *J. Appl. Phys.* **1995**, *77*, 4795−4800.
(31) Mollwo, E.; Muller, G.; Wagner, P. Energetische Lage Des Cu-Akzeptorniveaus in ZnO-Einkristallen. *Solid State Commun.* **1973**, *13*, 1283−1287.
(32) Kanai, Y. Admittance Spectroscopy of Cu-Doped ZnO Crystals. *Jpn. J. Appl. Phys.* **1991**, *30*, 703−707.
(33) Xu, C. X.; Sun, X. W.; Zhang, X. H.; Ke, L.; Chua, S. J. Photoluminescent Properties of Copper-Doped Zinc Oxide Nanowires. *Nanotechnology* **2004**, *15*, 856−861.
(34) Lee, S. Y.; Mettlach, N.; Ngugen, N.; Sun, Y. M.; White, J. M. Copper Oxide Reduction through Vacuum Annealing. *Appl. Surf. Sci.* **2003**, *206*, 102−109.
(35) Damen, T. C.; Porto, S. P. S.; Tell, B. Raman Effect in Zinc Oxide. *Phys. Rev.* **1966**, *142*, 570−574.
(36) Zhang, Z.; Huang, B.; Yu, Y.; Cui, D. Electrical Properties and Raman Spectra of Undoped and Al-Doped ZnO Thin Films by Metalorganic Vapor Phase Epitaxy. *Mater. Sci. Eng., B* **2001**, *86*, 109−112.
(37) Koyano, M.; QuocBao, P.; ThanhBinh, L. T.; HongHa, L.; NgocLong, N.; Katayama, S. I. Photoluminescence and Raman Spectra of ZnO Thin Films by Charged Liquid Cluster Beam Technique. *Phys. Status Solidi A* **2002**, *193*, 125−131.
(38) Hopfield, J. J.; Thomas, D. G. Fine Structure and Magneto-Optic Effects in the Exciton Spectrum of Cadmium Sulfide. *Phys. Rev.* **1961**, *122*, 35−52.
(39) Reynolds, D. C.; Look, D. C.; Jobai, B.; Litton, C. W.; Collins, T. C.; Harsch, W.; Cantwell, G. Neutral-Donor−Bound-Exciton Complexes in ZnO Crystals. *Phys. Rev. B: Condens. Matter Mater. Phys.* **1998**, *57*, 12151−15155.
(40) Leiter, F. H.; Alves, H. R.; Hofstaetter, A.; Hoffmann, D. M.; Meyer, B. K. The Oxygen Vacancy as the Origin of a Green Emission in Undoped ZnO. *Phys. Status Solidi B* **2001**, *226*, R4−R5.
(41) Gruzintsev, A. N.; Volkoiv, V. T.; Khodos, I. I.; Nikiforova, T. V.; Koval'chuk, M. N. Luminescent Properties of ZnO Films Doped with Group-IB Acceptors. *Russ. Microelectron.* **2002**, *31*, 200−205.
(42) Kohan, A. F.; Ceder, G.; Morgan, D.; Van de Walle, C. G. First-Principles Study of Native Point Defects in ZnO. *Phys. Rev. B: Condens. Matter Mater. Phys.* **2000**, *61*, 15019−15027.
(43) Tamura, K.; Makino, T.; Tsukazaki, A.; Sumiya, M.; Fuke, S.; Furumochi, T.; Lippmaa, M.; Chia, C. H.; Segawa, Y.; Koinuma, H.; Kawasaki, M. Donor−Acceptor Pair Luminescence in Nitrogen-Doped ZnO Films Grown on Lattice-Matched $ScAlMgO_4$ (0001) Substrates. *Solid State Commun.* **2003**, *127*, 265−269.
(44) Meyer, B. K.; Alves, H.; Hofmann, D. M.; Kriegseis, W.; Forster, D.; Bertram, F.; Christen, J.; Hoffmann, A.; Straßburg, M.; Dworzak, M.; Haboeck, U.; Rodina, A. V. Bound Exciton and Donor−Acceptor Pair Recombinations in ZnO. *Phys. Status Solidi B* **2004**, *241*, 231−260.
(45) Leroux, M.; Grandjean, N.; Beaumont, B.; Nataf, G.; Semond, F.; Massies, J.; Gibart, P. Temperature Quenching of Photoluminescence Intensities in Undoped and Doped GaN. *J. Appl. Phys.* **1999**, *86*, 3721−3728.
(46) Xiu, F. X.; Yang, Z.; Mandalapu, L. J.; Zhao, D. T.; Liu, J. L. Photoluminescence Study of Sb-Doped p-Type ZnO Films by Molecular-Beam Epitaxy. *Appl. Phys. Lett.* **2005**, *87*, 252102-(1−3).

DOI: 10.1021/acsami.5b01564
ACS Appl. Mater. Interfaces 2015, 7, 8894−8899